Geophys. J. Int. (2008) **174,** 904–918 doi: 10.1111/j.1365-246X.2008.03634.x

Coulomb stress evolution in Northeastern Caribbean over the past 250 years due to coseismic, postseismic and interseismic deformation

Syed Tabrez Ali,[1] Andrew M. Freed,[1] Eric Calais,[1] David M. Manaker[1,*] and William R. McCann[2]

[1]*Department of Earth and Atmospheric Sciences, Purdue University,* 550 *Stadium Mall Dr, West Lafayette,* IN 47907*, USA. E-mail: stali@purdue.edu*
[2]*Earth Scientific Consultants,* 10210 *West* 102nd *Ave, Westminster,* CO 80021*, USA*

Accepted 2007 September 24. Received 2007 September 19; in original form 2007 July 21

SUMMARY

The Northeastern Caribbean region accommodates ∼20 mm yr^{-1} of oblique convergence between the North American and Caribbean plates, which is distributed between the subduction interface and major strike-slip faults within the overriding plate. As a result, this heavily populated region has experienced eleven large ($M \geq 7.0$) earthquakes over the past 250 yr. In an effort to improve our understanding of the location and timing of these earthquakes, with an eye to understand where current seismic hazards may be greatest, we calculate the evolution of Coulomb stress on the major faults since 1751 due to coseismic, postseismic, and interseismic deformation. Our results quantify how earthquakes serve to relieve stress accumulated due to interseismic loading and how fault systems communicate with each other, serving both to advance or retard subsequent events. We find that the observed progressive westwards propagation of earthquakes on the Septentrional and Enriquillo strike-slip faults and along the megathrust was encouraged by coseismic stress changes associated with prior earthquakes. For the strike-slip faults, the loading of adjacent segments was further amplified by postseismic relaxation of a viscoelastic mantle in the decades following each event. Furthermore, earthquakes on the Septentrional fault relieve a small level of Coulomb stress on the parallel Enriquillo fault to the south (and vice versa), perhaps explaining anticorrelated timing of events on these respective fault systems. The greatest net build-up of Coulomb stress changes over the past 250 yr occurs along the central and eastern segment of the Septentrional and the Bowin strike-slip faults (65°–71°W), as no recent earthquake has relieved stress in these regions. For oblique thrust faults, net stress build-up over the past 250 yr is the largest on the North American/Caribbean megathrust west of 70.5°W. High Coulomb stress has also developed east of 65.5°W, where no historic events have been inferred to have relieved stress, though uncertainties in fault slip rates from our block model associated with a lack of GPS observations in this region may have led to an over-estimation of stress changes.

Key words: Earthquake interaction, forecasting, and prediction.

1 INTRODUCTION

The Northeastern (NE) Caribbean marks the active boundary between the North American and Caribbean plates, with ∼20 mm yr^{-1} of highly oblique relative plate convergence (Fig. 1). The region has among the highest population densities in the world (21.5 million on Hispaniola and Puerto Rico) concentrated on a seismogenic plate boundary. It has experienced at least eleven large ($M \geq 7.0$) earthquakes over the past 250 yr (Scherer 1912; Kelleher *et al.* 1973; McCann 2006), mostly distributed on the oblique subduction contact between the Caribbean and North American plates and on two major strike-slip fault systems within the overriding plate (Fig. 2, Table 1). These events show evidence for time–space progression on the strike-slip Septentrional (1842, 1887) and Enriquillo (1751b, 1770) faults and along the megathrust (1787, 1943, 1946, 1953 and 2003), suggesting a possible triggering relationship amongst earthquakes within each fault system. The alternate timing of events on the Enriquillo (18th century) and Septentrional (19th century) faults also suggests activity on one may temporarily suppress activity on the other (Dolan & Wald 1998). Understanding why earthquake sequences occur and the communication of stress between fault systems may hold the key to estimate seismic hazards in the NE Caribbean region.

*Now at: BP America, 501 Westlake Park Blvd., Houston, TX 77079, USA.

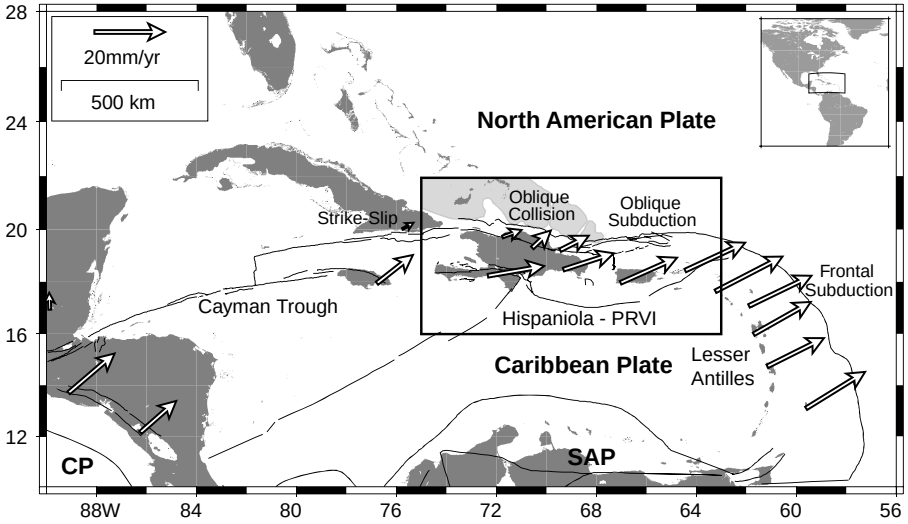

Figure 1. NE Caribbean region and surrounding tectonic setting. White arrows show a subset of available GPS measurements. Fault traces are represented by thin black lines. The colliding Bahama platform is shown in light grey. CP, Cocos Plate; SAP, South American Plate; PRVI, Puerto Rico Virgin Islands. Box shows the area covered in Figure 2.

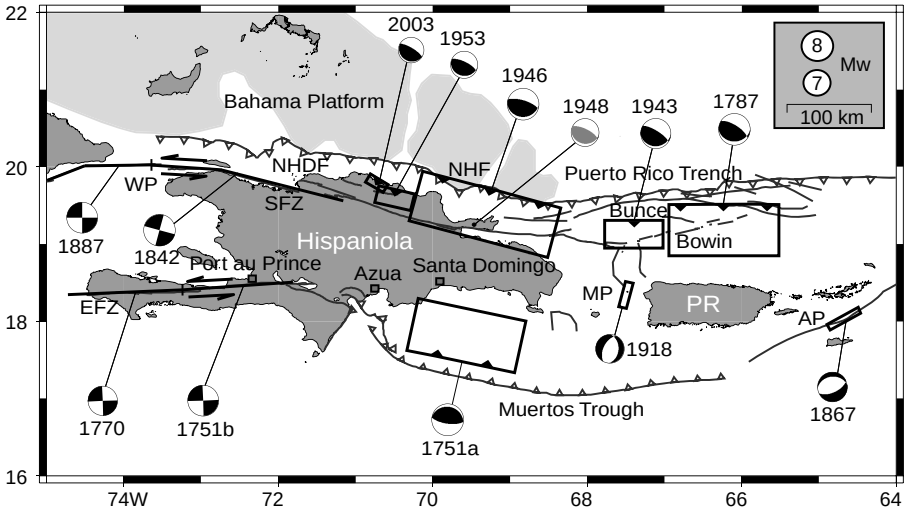

Figure 2. Map showing the focal mechanism and surface projection of estimated rupture planes/geometry for large ($M > 7.0$) historic and a recent $M6.5$ earthquake in the region since 1751. NHDF, North Hispaniola Deformation Front; NHF, North Hispaniola Fault; WP, Windward Passage; EFZ, Enriquillo Fault Zone; SFZ, Septentrional Fault Zone; MP, Mona Passage; PR, Puerto Rico.

Numerous studies have sought to understand the distribution of large earthquakes in space and time as a function of the evolution of crustal stresses (e.g. Deng & Sykes 1997; Freed *et al.* 2007). In a process referred to as 'earthquake triggering', earthquakes have been theorized to encourage or retard subsequent events in a region (see reviews by Stein 1999, 2003; King & Cocco 2001; Freed 2005). In some regions, large earthquakes appear to be explained simply by knowing how stress has changed over the past century or two due to earthquake slip and interseismic loading (e.g. Stein *et al.* 1997). No knowledge of the stress field prior to these relatively short periods is required. Stress evolution studies are usually cast in terms of Coulomb stress changes, which considers shear and normal stress changes to quantify whether faults have been pushed closer to (positive Coulomb stress change) or further away from (negative Coulomb stress change) failure by nearby earthquakes (e.g. Jaeger & Cook 1979; Stein & Lisowski 1983; King *et al.* 1994). Calculations of coseismic Coulomb stress changes have shown a correspondence with aftershock distributions (Reasenberg & Simpson 1992; Hardebeck *et al.* 1998; Toda *et al.* 1998; Parsons *et al.* 1999; Wyss & Wiemer 2000), earthquake sequences (Stein *et al.* 1994; Hodgkinson *et al.* 1996; Nostro *et al.* 1997; Nalbant *et al.* 1998) and seismic quiescence (Scholz 1998; Harris & Simpson 1996, 1998). In subduction zone settings, Taylor *et al.* (1998) found that earthquakes in the upper plate correlate with Coulomb stress increases induced by large interplate events. Lin & Stein (2004) found that 75 per cent of aftershocks following the 1960 $M9.5$ Valdivia (Chile) earthquake (including two $M \geq 7.0$ events) and 82 per cent of aftershocks following the $M8.1$ Antofagasta (Chile) earthquake occurred in regions brought closer to failure by the main shock.

In addition to coseismic Coulomb stress changes, postseismic relaxation of a viscoelastic lower crust and/or upper mantle, following major earthquakes can transfer significant stress upward to the seismogenic crust (e.g. Pollitz 1995; Freed & Lin 1998; Chery

Table 1. Location and source parameters of earthquakes considered in this study. Latitude (Lat.) and longitude (Lon.) refer to the estimated location.

Year (Month/Day)	Location	Long.	Lat.	M_w	Strike	Dip	Rake	Type	Length	Width	Slip
1751a (10/18)	S Hispaniola (MT)	70.00[m]	18.50[m]	8.0[m]	282	11[l]	90	TH	150	75	3.5
1751b (11/21)	S Hispaniola (EFZ)	72.00[m]	18.50[m]	7.5[m]	87.5	90	0	LL	150	20	3.0
1770 (06/03)	SW Hispaniola	73.50[m]	18.35[m]	7.5[m]	87.5	90	0	LL	150	20	3.0
1787 (05/02)	Puerto Rico Tr.	66.00[m]	19.25[m]	8.0[m]	90	25	60	TH	150	75	3.5
1842 (05/07)	N Hispaniola	72.50[m]	19.80[m]	8.0[m]	105	90	0	LL	300[d]	20	5.0
1867 (11/18)	Anegada Passage	65.00[m]	18.00[m]	7.3[m]	60	67*	−106*	N	50	20	3.0
1887 (09/23)	N Hispaniola	74.00[m]	20.00[m]	7.75[m]	90	90	0	LL	150	20	5.0
1918 (10/11)	C Mona Passage	67.62[dd]	18.28[dd]	7.2[dd]	207[dd]	54[dd]	−127[dd]	N	36[dd]	20	3.0
1943 (07/29)	N Mona Passage	66.95[d]	18.99[d]	7.88s[d]	90	19	60[d]	TH	80[d]	40[d]	2.0
1946 (08/04)	NE Hispaniola	68.94[D]	18.92[D]	8.1s[D]	102	22	76[D]	TH	195[D]	95[D]	3.75
1953 (05/31)	Silver Spur	70.40[D]	19.68[D]	7.0s[D]	100	20	75[D]	TH	40[D]	20[D]	0.75
2003 (09/22)	Puerto Plata	70.65[C]	19.90[C]	6.5	121[C]	15[C]	90[C]	TH	25[C]	15[C]	0.50

Magnitudes are moment magnitudes unless followed by an 'S' which indicates a surface wave magnitude and is assumed to be equal to moment magnitude (Scordilis 2006; Wells & Coppersmith, 1994). Type refers to the sense of slip: TH, predominantly thrust fault; LL, Left-lateral strike-slip fault; N, Normal fault. Length, width and coseismic slip are estimated from empirical scaling laws and relationship of Wells & Coppersmith (1994) and Fujii & Matsu'ura (2000). Strike and dip unless referenced are based on geometry of a block model (Manaker *et al.* 2008). Rake angles unless referenced are based on geological evidence. Superscripts refer to the following references: m, McCann (2006); dd, Doser *et al.* (2004); d, Dolan & Wald (1998) and/or Dolan & Bowman (2004); c, Calais (unpublished report); l, Ladd *et al.* (1977); *, based on CMT event 080193C.

et al. 2001; Marsan & Bean 2003). A number of studies have shown that such stress transfer may have a broad impact on the evolution of the regional stress field (e.g. Pollitz *et al.* 2003, 2005; Smith & Sandwell 2006; Freed *et al.* 2007). For example, stress increases at the eventual hypocentre of the 1999 Hector Mine, California earthquake induced by viscoelastic relaxation, following the nearby 1992 Landers quake may have influenced the relatively short time interval between these events (Freed & Lin 2001; Zeng 2001; Pollitz & Sacks 2002). Pollitz & Sacks (1997) inferred that Coulomb stress decreases associated with viscoelastic relaxation following the 1944 Tonankai and 1946 Nankaido earthquakes might have triggered the 1995 Kobe earthquake, by slowly unloading the normal stress on the fault (see also Hyodo & Hirahara 2004). Chery *et al.* (2001) attributed the clustering of three $M > 8.0$ earthquakes in Mongolia between 1905–1957, which occurred more than 400 km apart, to viscoelastic relaxation. Casarotti & Piersanti (2003) have suggested that negative Coulomb stress changes caused by postseismic stress diffusion associated with large subduction earthquakes in the 1900s may explain seismic gaps in Southern Peru and Northern Chile.

Previous studies have illuminated some of the stress interaction that may be occurring on the NE Caribbean plate interface. tenBrink & Lin (2004) showed how nearly trench parallel slip on the Puerto Rico subduction interface leads to strain partitioning by the strike-slip Bunce fault located less than 15 km from the trench, whereas the more normal subduction beneath Hispaniola leads to partitioning by the strike-slip Septentrional fault more than 60 km from the trench. Dolan & Bowman (2004) showed that each earthquake within the 1943–2003 subduction earthquake sequence was encouraged by the previous event and also increased Coulomb stresses on the eastern portion of Septentrional fault, which has not recently ruptured.

Here we consider how stress in the NE Caribbean has been modified by coseismic slip from eleven $M \geq 7.0$ events since 1751 (all known large events in this time period, Table 1) associated postseismic viscoelastic relaxation of the mantle, and interseismic strain accumulation resulting from the convergent Caribbean/North American plate margin. The objective is to understand how Coulomb stress in NE Caribbean has evolved over the past 250 yr and how these stress changes relate to historic seismicity. We are particularly interested in understanding what factors influence earthquake sequences within individual fault systems and how these fault systems communicate stress with each other. This study will help identify faults that have experienced the largest build-up of unrelieved stress over the past several centuries, which may point to regions of greatest seismic hazard.

2 TECTONIC SETTING

The NE Caribbean region marks the tectonic transition between frontal subduction of the North American plate beneath the Caribbean plate in the Lesser Antilles and roughly east–west strike-slip motion along the Cayman Trough (Fig. 1). GPS studies show that the interior of the Caribbean plate moves east–northeastwards (N70°E) at a rate of 18–20 mm yr^{-1} relative to the North American plate (DeMets *et al.* 2000), implying oblique convergence between the islands of Hispaniola and Puerto Rico on the Caribbean plate and the oceanic lithosphere of the North American plate.

Embedded in the plate boundary zone, the Puerto Rico-Virgin Islands (PRVI) block shows little to no internal deformation (Mann *et al.* 2002; Jansma *et al.* 2005). It overthrusts the North American oceanic lithosphere along the shallowly dipping Puerto Rico subduction, continuous to the east with the Lesser Antilles subduction. The northern Puerto Rico margin is also marked by two active strike-slip faults (Bunce & Bowin faults; tenBrink & Lin 2004; Grindlay *et al.* 2005), with unknown slip rates, that connect further west with the Septentrional fault (Fig. 2). At its southern boundary, the PRVI block overthrusts the Caribbean oceanic lithosphere along the low-angle Muertos thrust, active in its western half but with no evidence for active underthrusting east of 65°W (Byrne *et al.* 1985; Masson & Scanlon 1991). GPS measurements show 2–3 mm yr^{-1} of east–west extension between PRVI and Hispaniola (Jansma *et al.* 2000), accommodated by active extension in the Mona Passage (vanGestel *et al.* 1998). The boundary between PRVI and the Lesser Antilles is marked by the Anegada passage, which combines extension and strike-slip faulting (Lithgow *et al.* 1987).

West of the Mona Passage, the 22–27 km thick crust of the Bahama platform, carried by the North American plate, collides obliquely with the Caribbean margin along northern Hispaniola (Dillon *et al.* 1992; Dolan *et al.* 1998; Mann *et al.* 2002). Oblique convergence between the Caribbean and North American plates is partitioned between low-angle thrusting on the North Hispaniola fault and strike-slip faulting in the overriding plate on the

left-lateral Septentrional and Enriquillo faults (Calais *et al.* 2002). GPS and palaeoseismological data show that the Septentrional fault is currently slipping at about 7–10 mm yr^{-1} (Prentice *et al.* 2003; Manaker *et al.* 2008) and may be in the later part of its rupture cycle (Calais *et al.* 2002). Slip rate on the Enriquillo fault, although less well constrained, is on the order of $\sim$7 mm yr^{-1} (Manaker *et al.*, 2008). GPS measurements indicate elastic strain accumulation on the plate interface along Hispaniola (Dixon *et al.* 1998; Mann *et al.* 2002), with interplate coupling decreasing to the east (Manaker *et al.*, 2008). West of Hispaniola, the North Hispaniola fault gradually decays out and ends at the longitude of the Windward Passage, where the Caribbean–North American plate motion transitions to pure strike-slip.

3 EARTHQUAKE CATALOGUE

Reports of earthquakes in the Greater Antilles date as far back as the sixteenth century when the region was being colonized by the Spanish. Salterain (1883) and Taber (1922) were among the first to systematically catalogue and report significant seismic events in the NE Caribbean. Later work by Kelleher *et al.* (1973) continued to refine the catalogue of historical events in the region. Here, we use earthquake locations and magnitudes from the Instituto Panamericano de Geografía e Historia (IPGH) catalogue (Tanner & Shepherd 1997) as summarized by McCann (2006), specially for the pre-1900 earthquakes and follow Doser *et al.* (2005), Dolan & Wald (1998), Ladd *et al.* (1977) and the Harvard Centroid Moment Tensor (CMT) catalogue for the post-1900 earthquakes. Events are sparse before 1750, when settlers started spreading across the islands and developing a consistent written record of felt events. As early events (pre-1900) are very poorly located, we use the current knowledge of the regional geology and active faults, as well as damage reports, to assign a location to historical events. We use the inferred magnitudes together with the empirical scaling laws and relationships of Wells & Coppersmith (1994) and Fujii & Matsu'ura (2000) to estimate rupture areas and amount of slip. Strike, rake and dip are based on the fault geometry from geological observations and/or focal mechanism of recent events on that fault. In the absence of well-constrained coseismic slip distributions, the earthquakes are modelled as rectangular planar patches with uniform slip and are assumed to occur within a 30 km thick elastic crust. Deeper events (such as the 1948 earthquake that occurred below the 1946 rupture plane, Dolan & Wald 1998) are not considered in our analysis as deformation beneath 30 km is assumed to be viscoelastic. The source parameters associated with all eleven $M \geq 7.0$ (and one recent M6.5) earthquakes considered in the present analyses are shown in Table 1 and Fig. 2.

The first event we consider is the 1751 Southern Hispaniola earthquake (1751a in Table 1) that is inferred to have occurred on the shallowly north dipping Muertos Trough subduction interface (McCann & Sykes 1984; McCann 2006). We use a strike of 282°, consistent with the strike of the trench and geometry of the block model (Manaker *et al.*, 2008), an average dip of 11° (Ladd *et al.* 1977), and a rake of 90° (close to the 92° rake angle for the 1984 M6.7 earthquake beneath Muertos Trough; Byrne *et al.* 1985). Using empirical scaling laws we estimate a rupture area of 150 × 75 km and average slip of 3.5 m. Following the 1751 October 18 earthquake, a major aftershock (1751b in Table 1) is documented in the historic record (Scherer 1912). We follow the inference that this M7.5 event occurred on the left-lateral eastern Enriquillo fault (McCann 2006; Dolan & Wald 1998), assuming a rupture depth from 0–20 km, a rupture length of 150 km, and an average slip of 3 m (based on empirical scaling laws). The M7.5 earthquake in 1770 is inferred to have occurred in Southern Hispaniola (Scherer 1912) on the western Enriquillo fault, extending the 1751b rupture (Dolan & Wald 1998). We assume that the earthquake was similar in size (and sense of slip) to the 1751b earthquake. A M8.0 earthquake in 1787 has been proposed on the thrust interface offshore Puerto Rico (McCann 1985, 2006). Based on the geometry of the subduction interface in the block model and empirical scaling laws, we estimate a rupture area of 150 × 75 km and a uniform average slip of 3.5 m. We assume a rake angle of 63° based on average slip vectors of recent M5.0–6.0 earthquakes in the region (Doser *et al.* 2005).

The next major event in the region is the 1842 M8.0 earthquake in northwest Hispaniola. It is one of the largest historic earthquakes to have occurred on the Island, rupturing a 300 km-long portion of the western Septentrional fault (Mann *et al.* 1998). Based on empirical scaling laws, we model the rupture as 20 km wide with an average slip of 5 m. A M7.3 normal faulting earthquake (incorrectly identified as a M7.5 event in the IPGH catalogue and in McCann 2006) in 1867 is known to have occurred in Anegada Passage (Reid & Taber 1920; McCann 1985, 2006). Based on empirical scaling laws and on the focal mechanism of a 1993 M5.2 earthquake in the region (CMT catalogue), we estimate a rupture area of 50 × 20 km, a strike of 60° (both consistent with the geometry of the block model), and dip and rake angles of 67°and –106°, respectively. The 1887 M7.8 earthquake is inferred to have occurred on the western Septentrional fault, thereby extending the 1842 rupture. Based on scaling laws, we estimate a rupture area of 175 × 20 km and an average slip of 5 m for this event.

The 1918 normal faulting earthquake in the Mona Passage (Reid & Taber 1919) ruptured two 18 km long patches accommodating 3 m of average slip (Doser *et al.* 2005). The 1943–1953 sequence of earthquakes has been discussed in detail by Dolan & Wald (1998); however, their moment magnitudes (M_S) are based on Kelleher *et al.* (1973) who used magnitudes as given by Gutenberg & Richter (1954) and Rothe (1969). For our calculations we use the corrected magnitudes of Pacheco & Sykes (1992), consistent with the IPGH catalogue. The 1943 M_S7.5 (M_S7.8 in Dolan & Wald 1998) earthquake ruptured a 80 × 40 km segment below northeastern Mona Passage with an inferred oblique rake of $\sim$60° (Dolan & Bowman 2004). Based on scaling laws we estimate an average slip of 2.0 m for this event. The magnitude as well as the mechanism of the 1946 earthquake is debated. According to Dolan & Wald (1998) the M_S8.1 earthquake (M_S7.8 in IPGH catalogue) occurred on the shallow dipping North Hispaniola fault and had an estimated rupture area of 195 × 95 km, coinciding with the limits of the Hispaniola–Bahama collision zone. However, according to Russo & Villasenor (1995), the 1946 main shock was a M_S7.8 event that occurred on a northwest striking, steeply dipping fault plane with significant left-lateral motion. For the stress evolution calculations, we model it as a M_S7.8 earthquake (consistent with the IPGH catalogue) and choose Dolan & Wald's (1998) focal mechanism as it is consistent with aftershock locations, considering the alternative interpretation as another end-member model. Following the 1946 main shock were two major aftershocks, a M_S7.4 (M_S7.8 in Dolan & Wald 1998) event on August 8 and a M_S7.0 event on October 4 (M_S6.1 in Russo & Villasenor 1995). The focal mechanism of the August 8 aftershock is not well constrained (Dolan & Wald 1998), and Dolan & Bowman (2004) suggest that this event does not significantly add to the stress changes induced by the main shock (regardless of which nodal plane is chosen). Since the average

magnitude of the Oct 4 aftershock is less than 7.0 and occurred at a depth of 35 km (Russo & Villasenor 1995) overlapping with the downdip limit of the 1946 main shock and extending it (Dolan & Wald 1998), we follow Dolan & Bowman (2004) and model the main shock as a single rectangular patch 195 × 95 km wide with a uniform slip of 3.75 m (consistent with scaling laws and the cumulative moment release).

The M_S7.0 earthquake in 1953 beneath northern Hispaniola occurred between depths of 15–25 km, and we estimate a rupture area of 40 × 20 km with a uniform slip of 0.75 m. For the 2003 M6.5 event, coseismic offsets from GPS data (Calais, unpublished report) suggest a shallow dipping pure thrust fault with a rupture length of 28 km between 1 and 4 km depth above the plate interface with a strike of 121°.

4 EVOLUTION OF STRESS

4.1 Method

We focus our study on the calculation of Coulomb stress changes, based on the concept of a critical Coulomb failure stress, σ_c, in which

$$\sigma_c = \tau - \mu(\sigma_n - p), \quad (1)$$

where τ is shear stress parallel to the slip direction of a fault, σ_n is fault-normal (or clamping) stress, p is pore fluid pressure and μ is the coefficient of friction (Jaeger & Cook 1979; Scholz 2002). As the absolute stress field is difficult to determine, we calculate stress changes over a period of time using the relation

$$\Delta\sigma_c = \Delta\tau - \mu\Delta\sigma_n, \quad (2)$$

where $\Delta\sigma_c$ represents change in stress and μ' is the apparent friction, which takes into account reductions in friction due to pore pressure changes. A positive Coulomb stress change implies that a fault is brought closer to failure, whereas a negative Coulomb stress change implies that a fault is brought farther away from failure. Here, we calculate the evolution of Coulomb stress in the NE Caribbean by considering contributions from coseismic, postseismic and interseismic deformation since the 1751 Muertos Trough earthquake. Stress changes due to each mechanism are solved separately and added together. Our objective is to determine the role of each of these mechanisms in the evolution of stress since 1751 and to determine how stress at subsequent hypocentres was influenced.

To calculate coseismic and postseismic stress changes, we use the method of Pollitz (1996, 1997) in which the spheroidal and toroidal modes of a spherically stratified viscoelastic earth (no lateral heterogeneity in viscosity or in the thickness of various layers) are computed and then used to calculate the deformation field. Fig. 3 shows the depth-dependent earth structure used in this study. Earthquake sources as described previously are listed in Table 1. Rupture surfaces that experience coseismic slip during the earthquake are assumed to remain locked at all other times. Coseismic stress changes within the hot lower crust and upper mantle cannot be sustained and lead to viscoelastic flow, which acts to transfer stress upwards to the seismogenic crust. Such stress transfer usually works to reload the fault, but can either increase or decrease coseismic Coulomb stress changes in the surrounding region, depending on the geometry and sense of slip of the earthquake and the candidate receiver fault. We assume that viscoelastic processes occur below 30 km depth, the maximum depth of the earthquakes considered in this analysis. Coseismic stresses above this depth are assumed to be maintained, which may lead to an underestimation of postseismic stress changes

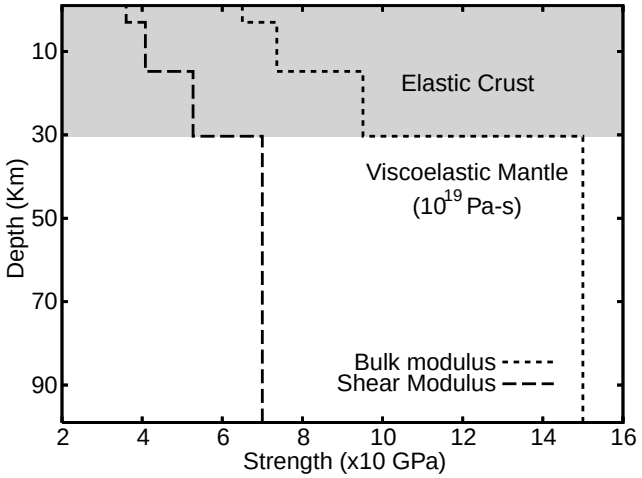

Figure 3. Assumed elastic and viscoelastic structure used in the model.

if significant flow above 30 km depth occurs, for example, within the lower crust between 20 and 30 km depth. We assume a viscosity of 10^{19} Pa s, based on the average inferred effective viscosity of the mantle in the decades following large subduction earthquakes (Wang *et al.* 2001; Hu *et al.* 2004; Khazaradze *et al.* 2002; Lorenzo-Martin *et al.* 2006).

Interseismic deformation is modelled using backslip (Savage 1983) where the results from a freely sliding interplate boundary are superimposed with a dislocation solution coinciding with the seismogenic zone slipping in the opposite direction (known as 'backslip'). To a first order, especially over a period of a few hundred years, the aseismic slip portion of this calculation does not contribute to the regional stress field. Thus, interseismic stress is calculated using only the backslip component. The backslip rate can be thought of as a slip deficit rate, which, when multiplied by a time interval, represents the amount of slip that will eventually have to be accommodated by earthquakes. We use the slip deficit rates (associated with the North American/Caribbean plate interface, the Septentrional and Enriquillo strike-slip faults and the Muertos Trench) computed by the block model of Manaker *et al.* (2008) that uses GPS, geological and earthquake slip vector data to estimate block motions and coupling ratios (0 corresponds to a fully creeping fault, 1 corresponds to a fully locked fault) along the major NE Caribbean faults.

Fig. 4 and Table 2 show the slip deficit rates inferred from the block model as interpolated to the fault geometry we assume in our study (locking depth, dip angle and slip deficit rates for each segment

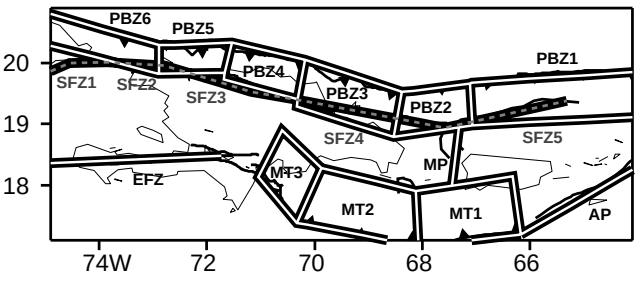

Figure 4. Fault geometry used to calculate interseismic stress rates. Slip deficit rates and locking depths are summarized in Table 2. PBZ, Plate boundary zone; SFZ, Septentrional fault zone; EFZ, Enriquillo fault zone; MT, Muertos Trough; AP, Anegada Passage; MP, Mona Passage.

Table 2. Local slip deficit rates, locking depths and dip angles for segments used to calculate interseismic stress rates. Segment numbers refer to those shown in Figure 4. LL: local left-lateral component; TH: local thrust component.

Fault segment (see Fig. 4)	Locking depth (km)	Dip angle (deg.)	Slip deficit (mm yr^{-1})	
			LL	TH
PBZ1	30	20	−4.17	−2.18
PBZ2	30	20	−3.02	−2.39
PBZ3	30	20	−1.88	−2.60
PBZ4	25	20	−1.79	−3.69
PBZ5	20	20	−2.76	−3.62
PBZ6	20	20	−2.48	−2.90
SFZ1-SFZ5	20	90	−7.00	0.00
EFZ	20	90	−7.00	0.00
MT1	30	15	−1.97	−1.85
MT2	30	15	−4.00	−2.78
MT3	30	15	−5.00	−2.74
MP	20	60	−4.58	10.0
AP	20	60	−0.5	3.00

are summarized in Table 2). Interseismic stressing rates are obtained by applying the slip deficit rate as slipping fault patches, using the same method as used for the coseismic calculations. The geometry of the subduction interface as well as that of the strike-slip faults is consistent with that used in the block model of Manaker *et al.* (2008). The averaged slip deficit rates for the interplate subduction, and the Muertos Trough thrust interface range from 3.0 to 5.0 mm yr^{-1}. In contrast both the Enriquillo and Septentrional strike-slip faults slip at a relatively higher rate of 7.0 mm yr^{-1} that corresponds to an average slip deficit of 1.75 m over 250 yr. To calculate stress changes resulting from long term extension in Mona and Anegada Passage, we model the two areas as 60° dipping normal faults, the average dip of recent earthquakes in the region. Though these areas comprise numerous, small, active faults, we assume that extension is taken up by one major fault as shown in Fig. 4. The block model estimates 5 mm yr^{-1} of horizontal extension in the Mona Passage and 1.5 mm yr^{-1} in the Anegada Passage, which on a 60° dipping normal fault corresponds to slip deficit rates of 10 and 3 mm yr^{-1}, respectively.

To calculate Coulomb stress magnitudes, we assume a relatively low apparent friction of 0.2 for strike-slip faults and a relatively high apparent friction of 0.8 for thrust faults. These friction coefficient values are consistent with previous studies in which aftershock patterns following thrust earthquakes appear to be more sensitive to normal stress changes, suggesting a higher friction coefficient (Stein & Ekstrom 1992; Shearer 1997; Hardebeck *et al.* 1998; Parsons *et al.* 1999), whereas strike-slip faults are inferred to be associated more with shear stress changes corresponding to a lower effective friction value (Zoback *et al.* 1987; Parsons *et al.* 1999; Toda & Stein 2002). For normal faults we assume a friction coefficient of 0.6 as estimated from fault reactivation studies (Collettini & Sibson 2001). Subsequent sections describe the calculated Coulomb stress changes associated with each mechanism, followed by a discussion of combined stress changes.

4.2 Coseismic stress changes

Fig. 5 shows the calculated cumulative coseismic Coulomb stress change after each earthquake, using the component of stress associated with the fault orientation and slip direction of the next event. Though perhaps surprising considering the short time span between events, Fig. 5a shows that stress changes associated with the 1751a Muertos Trough event had insignificant influence (<0.1 MPa increase) on the eastern Enriquillo fault which ruptured only 34 days later (1751b). Though Scherer (1912) assumed that the latter event was an aftershock of the earlier event, a reasonable conclusion considering the short delay time and relatively short distance between events, our results suggest that coseismic Coulomb stress change following the 1751a event, as modelled, does not satisfactorily explain the triggering of the Enriquillo earthquake. However, if the rupture plane of the ill-constrained offshore Muertos Trough earthquake is slightly shifted towards the west, then the triggering of the 1751b earthquake seems plausible. Though the location of the modelled slip may be in error, this may also be evidence of the importance of dynamic stress changes associated with the passage of transient seismic waves to trigger subsequent events (e.g. Gomberg 1996; Gomberg *et al.* 2003). In contrast, the 1751b earthquake that ruptured a large portion of the eastern Enriquillo fault increased stress (>0.1–1.6 MPa) on the 1770 rupture surface to the west (Fig. 5b).

The 1751a Muertos Trough rupture modestly increased stress (as much as 0.65 MPa) on the central Septentrional fault to the north, which has not ruptured in historic time (Fig. 5b). However, part of the western Septentrional fault, which ruptured in 1842, does not appear to have been significantly encouraged by the Enriquillo or Muertos Trough events (Fig. 5d). This is also the case for the 1787 Puerto Rico trench quake (Fig. 5c), suggesting that if either event was influenced by previous earthquakes, those events occurred prior to 1751. As with the Enriquillo sequence, the 1842 rupture on the Septentrional fault was followed by a rupture on the neighbouring segment in 1887, which was loaded (>0.1–1.6 MPa across its length) by the 1842 event (Fig. 5f).

The Puerto Rico trench earthquake in 1787 is the first major thrust earthquake in a sequence on the North American–Caribbean subduction interface that progresses to the west. The 1787 earthquake increased stress (>0.4–2.4 MPa) on the adjacent segment that ruptured in 1943 (Fig. 5h). The next event in the sequence, the 1946 NE Hispaniola earthquake occurred on the other side of a 75-km-wide gap and was encouraged by a relatively low stress change of ∼0.1 MPa (Fig. 5i), though the short time interval between events suggests that this small stress change may have been sufficient to influence the timing of the 1946 earthquake. The 1946 event greatly increased stress (>2.4 MPa) on the neighbouring segment that ruptured in 1953 (Fig. 5j). This event in turn encouraged (>1.6 MPa) the recent 2003 Puerto Plata quake (Fig. 5k).

Two historic normal faulting earthquakes have occurred in the region since 1751. The 1867 Anegada Passage earthquake was very modestly encouraged by the 1787 Puerto Rico Trench event on its southwestern edge (as much as 0.1 MPa) but slightly discouraged (as much as –0.1 MPa) on its northeastern edge (Fig. 5e). The 1918 normal faulting earthquake in central Mona Passage was encouraged (as much as 1.2 MPa) by both the 1787 plate interface quake to the north and the 1751 Muertos Trough event to the south (Fig. 5g).

Overall, of the 11 earthquakes that occurred after the 1751 Muertos Trough quake, six events occurred in regions that experienced previous coseismic stress changes of at least 0.1 MPa. The 1751b, 1787, 1842 and 1946 quakes occurred on fault segments where stress changes from preceding earthquakes were less than 0.1 MPa, though some these events may have been influenced by earthquakes that occurred prior to 1751. The 1867 event experienced slight Coulomb stress increase on its western edge and slight decrease on its eastern half. Unfortunately, the hypocentre of this event is

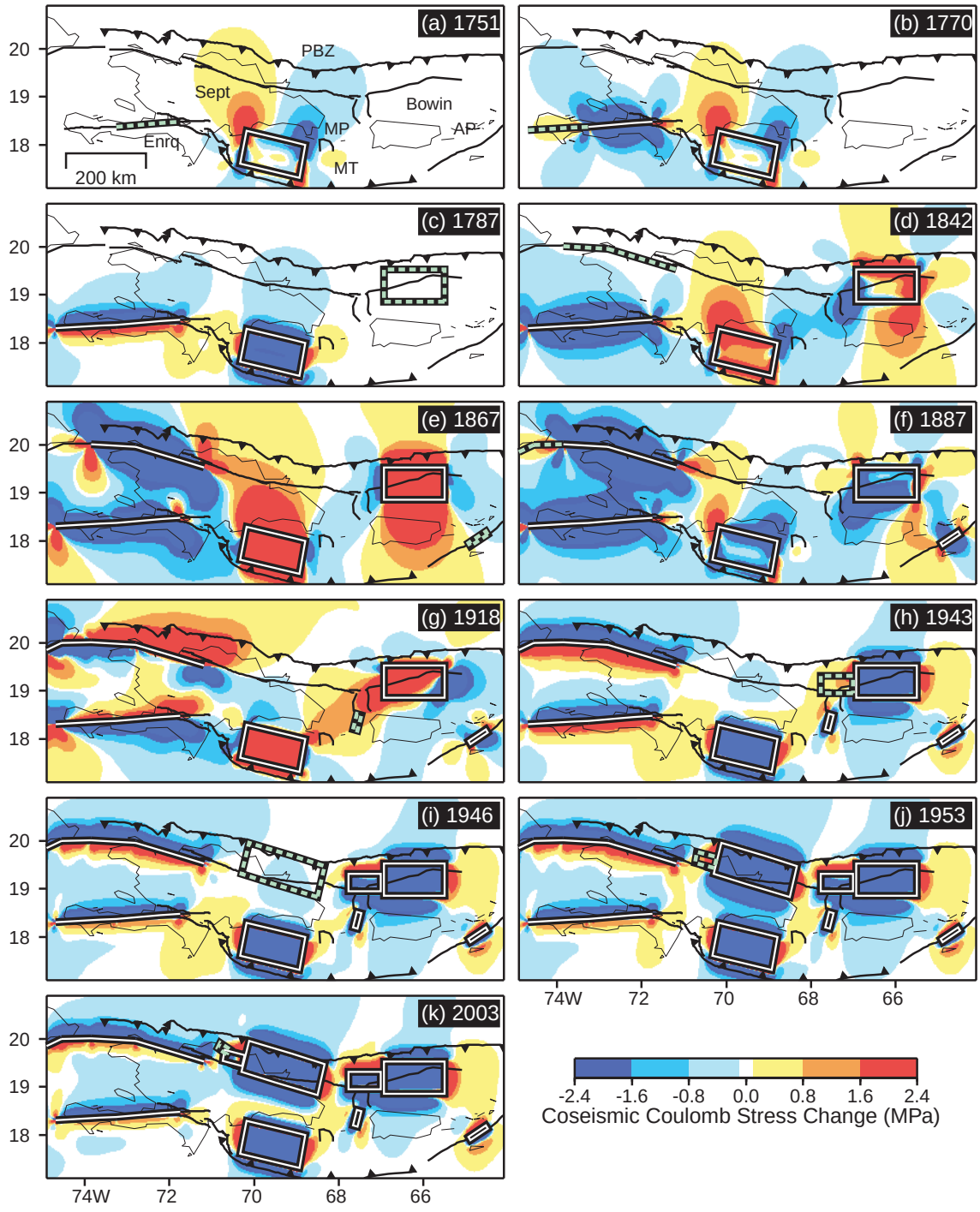

Figure 5. Coulomb stress change due to coseismic slip from all preceding earthquakes (white within black lines) as evaluated on the rupture plane of the earthquake about to occur (dashed green within black lines), highlighted in each panel. Stresses are shown for a depth of 15 km, the average depth of hypocentres for historic events (except for the 2003 earthquake, which had a hypocentral depth of ∼3 km). A friction coefficient of 0.2 is assumed for strike-slip earthquakes (panels a, b, d and f), 0.6 for normal faulting earthquakes (panels e and g) and 0.8 for thrust earthquakes (panels c, h, i, j and k). PBZ, Plate boundary zone; Sept, Septentrional fault; Enrq, Enriquillo fault; MT, Muertos Trough; AP, Anegada passage; MP, Mona passage.

not well constrained to help determine whether this event may have been triggered by the 1787 quake. Collectively, this suggests that coseismic stress changes appear to have had at least a moderate influence on the occurrence of subsequent events and may be a viable means of understanding current seismic hazard in the NE Caribbean region (discussed below).

4.3 Postseismic stress changes

Fig. 6 shows the evolution of Coulomb stress due to postseismic relaxation associated with each of the earthquakes considered. Each panel in the figure corresponds to the same panel in Fig. 5 (same Coulomb stress component) but shows the cumulative stress change

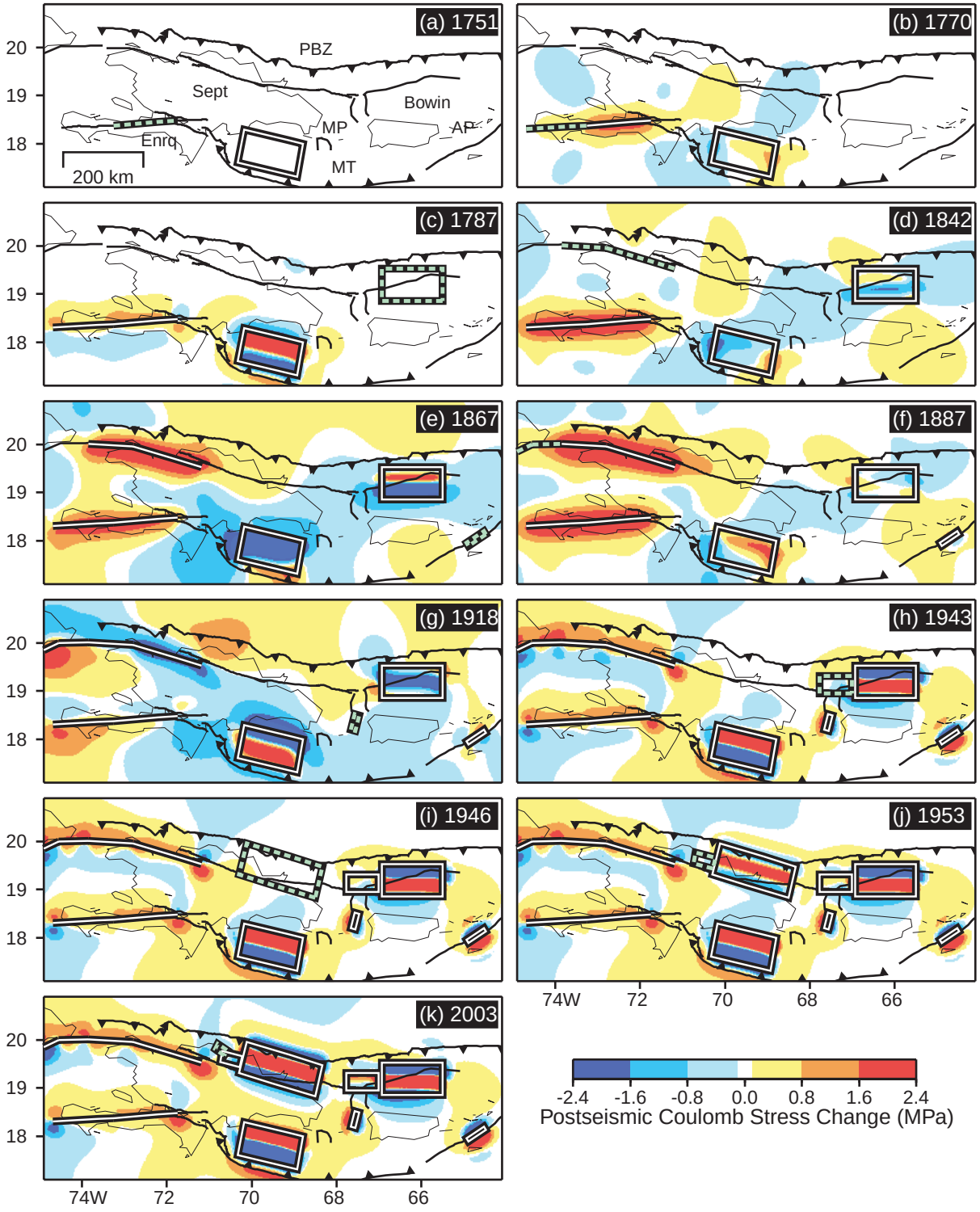

Figure 6. Same as Fig. 5 but for calculated Coulomb stress changes associated with postseismic relaxation following all earthquakes prior to the year of the next event highlighted in each panel. Fault labels are same as in Fig. 5.

solely due to postseismic relaxation from previous events. For a viscosity of 10^{19} Pa s, it takes ∼100 yr for 90 per cent of mantle coseismic stresses to be relaxed and transferred to the surface. Fig. 6a shows stress changes associated with 34 days of postseismic relaxation, following the 1751a Muertos Trough event (time period between the 1751a and 1751b events). Significant postseismic relaxation has not yet had time to occur, thus the calculated stress changes are negligible.

Results suggest that postseismic relaxation is an important contributor to the loading of adjacent segments following strike-slip earthquakes. Figs 6b and f show that postseismic relaxation following earthquakes on the Enriquillo and Septentrional faults works

to reload not only the rupture surfaces but also the adjacent segments that subsequently ruptured in both cases. Postseismic relaxation leads to Coulomb stress increases of as much as 0.8 MPa on the 1770 Enriquillo rupture plane and by as much as 1.5 MPa on 1887 Septentrional rupture plane. Loading of adjacent strike-slip segments by postseismic relaxation found in these calculations is similar to that found following large strike-slip events in southern California (Freed *et al.* 2007).

For the case of the sequence of thrust earthquakes along the North American/Caribbean plate interface, the role of postseismic relaxation is more complex. The 1943 interplate event was both encouraged (as much as 1.6 MPa on its eastern edge) and discouraged (by as much as –0.1 MPa toward its centre) by the 1787 interplate event, directly to the east (Fig. 6h). As the hypocentre of this offshore event is not well constrained, it is difficult to determine the role that postseismic relaxation may have had in triggering it. The 1946 North Hispaniola thrust event was located far from the 1943 event and the time period between events too short for postseismic relaxation to have played a significant role in its triggering (Fig. 6i). The 1953 (Fig. 6j) event also occurred directly adjacent to the previous rupture (the 1946 event) and again was both encouraged (as much as 0.1 MPa) and discouraged (–0.1 MPa) by Coulomb stress changes associated with the postseismic relaxation. Postseismic relaxation following the 1953 quake does not show any significant effect at the site of the shallow thrust 2003 earthquake.

The difference between the influence of postseismic stress changes on neighbouring segments of strike-slip earthquakes (always encourages) versus oblique thrust earthquakes (could encourage or discourage) is primarily due to the difference in dip angle between these two fault types. Fault dip along with the rake angle significantly influences the distribution of regions of positive and negative coseismic Coulomb stress changes in the mantle beneath. Coseismic slip associated with vertical (or near-vertical) strike-slip faults leads to lobes of Coulomb stress increases in the mantle beneath adjacent segments. When these regions relax, these stresses migrate to the seismogenic crust above and load the fault. In contrast, shallow dipping thrust faults lead to a more complex pattern of coseismic stress change with lobes of Coulomb stress both increase and lobes of stress decrease in the mantle beneath adjacent thrust segments, with the sign of the change being a function of depth. Thus, the relaxation of these regions leads to a transfer of stress to the seismogenic zone above that varies along strike, induce both loading and unloading along the adjacent segments. Understanding the influence of postseismic relaxation on the triggering of adjacent thrust segments thus requires well-constrained hypocentral locations. Unfortunately, these locations are not well constrained for most historic earthquakes in the region.

4.4 Interseismic stress changes

Coulomb stress changes due to 250 yr of interseismic stress build-up associated with each of the major fault systems in NE Caribbean, as resolved on N95°E striking (average strike angle) strike-slip faults, are shown in Fig. 7 (one panel for each of the major fault systems). These panels show how interseismic stresses work to load strike-slip faults in the region over time. If the sign of stress changes in the panels is reversed (i.e. red to blue and blue to red), these panels can be interpreted as showing how the complete rupture of these faults systems would unload stress in the region every 250 yr. This is because, to a first order, all interseismic stress accumulation in the upper crust must eventually be released by earthquakes.

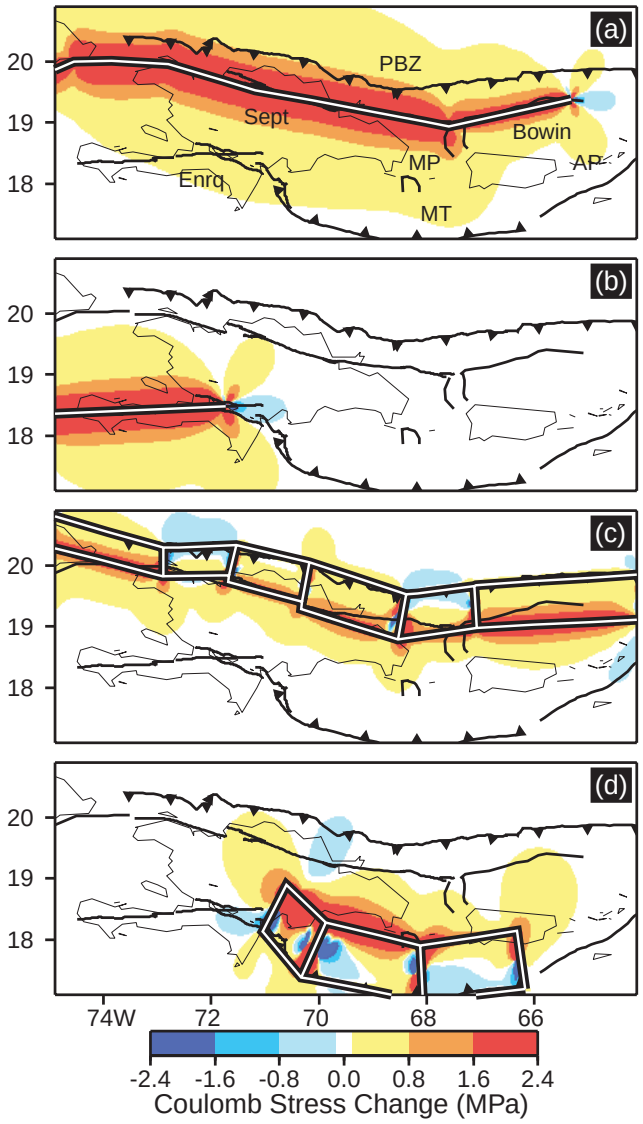

Figure 7. Coulomb stress changes resolved on N95°E striking left-lateral strike-slip faults due to 250 yr of interseismic stress build-up on the (a) Septentrional and Bowin Faults, (b) Enriquillo Fault, (c) North American/Caribbean plate boundary and (d) the Muertos Trough thrust interface. Stresses are resolved at a depth of 15 km with a friction of 0.2. Fault labels are same as in Fig. 5.

Fig. 7a shows that interseismic stressing rates load the locked 700 km long Septentrional fault and surrounding region, as well as part of the Enriquillo fault to the south. This figure can be interpreted as showing that earthquake sequences on the Septentrional fault tend to relieve stresses on the Enriquillo fault. Similarly, although not obvious, earthquakes on the Enriquillo fault slightly relieve stresses on the Septentrional fault. Although the magnitude of stress relief imparted by the Septentrional and Enriquillo faults through one earthquake cycle is relatively small, over the course of many earthquake cycles, this could be sufficient to cause earthquake activity on these fault systems to become anticorrelated. This may explain why the latest earthquakes on the Enriquillo occurred in the 18th century, whereas the latest events on the Septentrional occurred in the 19th century. Such interaction between two parallel strike-slip faults has also been observed in numerical experiments involving synthetic seismicity (Robinson & Benites 1995).

Fig. 7c shows that interseismic stress accumulation associated with the northern, oblique subduction plate boundary zone leads to efficient loading of the Septentrional and Bowin faults (assuming a friction coefficient of 0.2). This illustrates the mechanical relationship between thrusts and strike-slip faults at an obliquely convergent plate boundary. Coulomb stresses due to the locking of the north Hispaniola and Puerto Rico trench thrust fault system serve to load the Septentrional–Bowin strike-slip faults, especially from beneath where the shear is maximum. The partitioning of slip therefore appears to be favoured by the efficient transfer of Coulomb stresses to the upper plate. However, if we assume a high friction coefficient ($\sim$1.0) then oblique subduction in fact tends to decrease stress on the Septentrional fault, as normal stress changes dominate over shear stress changes. Such a result is counter-intuitive, as the Septentrional fault helps to partition some of deformation associated with oblique subduction. This suggests that major strike-slip faults are indeed best described by a relatively weak apparent friction. In a similar fashion, earthquakes on the thrust interface such as the 1946 NE Hispaniola earthquake, which on average tended to unload a low friction Septentrional, now tend to significantly load the fault if it is controlled by high friction.

Despite its distance to the south, interseismic stresses associated with the Muertos Trough have influence far to the north, in part due to the relative shallow dip (11°–15°) of this interface. Fig. 7d shows that interseismic loading associated with the Muertos Trough leads to high Coulomb stresses in Southeastern Hispaniola, encouraging left-lateral strike-slip faulting. This is because the long-term slip rate on Muertos Trough has a significant left-lateral component. However, absence of active left-lateral faults in Southeastern Hispaniola suggests that strain in this region is not partitioned, and earthquakes on the thrust interface may in fact have a high left-lateral component. The Muertos Trough also does not appear to influence stresses on the Enriquillo fault despite its close proximity.

Coulomb stress changes due to 250 yr of interseismic stress build-up associated with each of the major fault systems, as resolved on N95°E striking, oblique (67.5° rake) thrust faults, are shown in Fig. 8 (panels correspond to those in Fig. 7). These panels show how interseismic stresses work to load oblique thrust faults in the region over time. Fig. 8a shows that interseismic stress accumulation associated with the locked Septentrional and Bowin faults work to load the oblique subduction plate interface to the north. This is equivalent to showing that strike-slip earthquakes on these faults work to unload the Coulomb stresses that develop on the subduction interface. Fig. 8b shows stress accumulation/release associated with the Enriquillo fault to not have much of an influence on thrust faults in the region. Whereas the existence of the Septentrional and Bowin faults can partly be understood in terms of strain partitioning of oblique subduction between the Caribbean and North American plates, the Enriquillo fault appears to be located too far south to efficiently interact with the stress transfer associated with the strain partitioning. The Enriquillo fault most likely serves to accommodate the remaining of the Caribbean–North American shear motion not taken up by the Septentrional fault.

Fig. 8c shows that interseismic stresses due to the locking of the North America/Caribbean plate interface accumulate along that plate interface. Stresses are highest downdip as the edge of the locked (or partially locked) seismogenic zone is approached (though the figure must be interpreted with caution since it only shows stress at 15 km depth). Similarly, interseismic stresses associated with the Muertos Trough also lead to loading of the thrust component of this locked fault (Fig. 8d). Using a lower friction coefficient ($\sim$0.0)

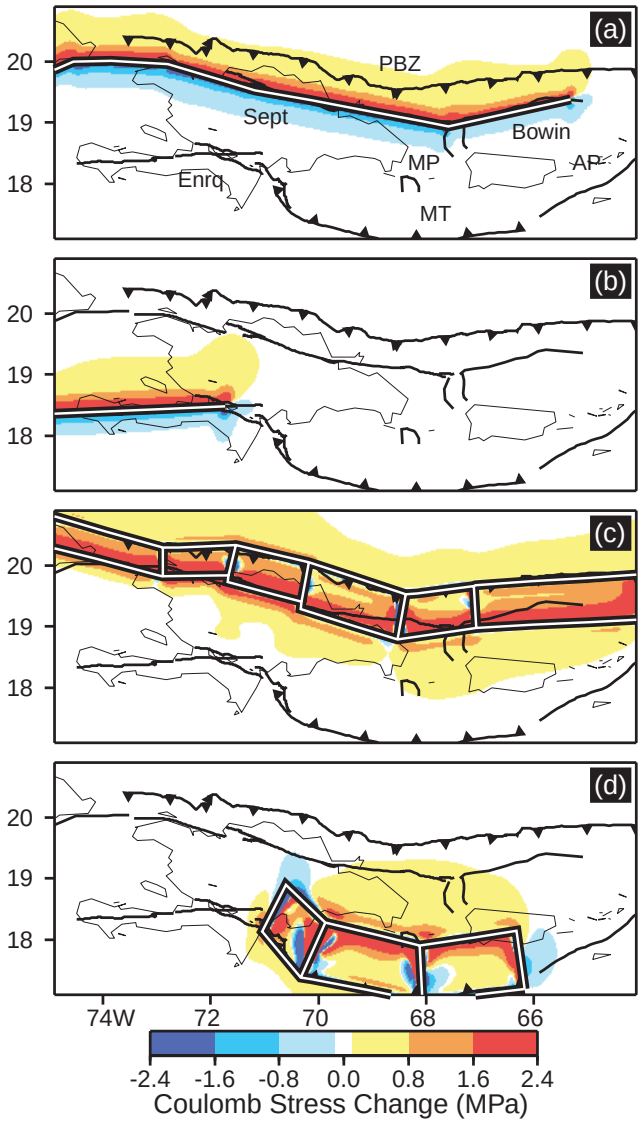

Figure 8. Coulomb stress changes resolved on N95°E striking oblique (rake of 67.5°) thrust faults due to 250 yr of interseismic stress build-up on the (a) Septentrional and Bowin Faults, (b) Enriquillo Fault, (c) North American/Caribbean plate boundary and (d) the Muertos Trough. Stresses are resolved at a depth of 15 km with a friction of 0.8. Fault labels are same as in Fig. 5.

has little effect on the magnitude and pattern of Coulomb stress change on the major thrust faults due to interseismic (or coseismic) deformation. This is because shear stress changes dominate over normal stress changes, regardless of the friction level.

4.5 Cumulative stress changes

Fig. 9 displays the cumulative stress changes as resolved on N95°E striking left-lateral strike-slip faults incurred in the region from 1751 to 2007 from each of the three mechanisms of the earthquake cycle, both individually and combined. The figure shows how the key components of the earthquake cycle contribute to driving the shear component of the stress field. Earthquakes release stress (blue regions) on strike-slip faults (Fig. 9a), whereas postseismic relaxation (Fig. 9b) and interseismic stressing (Fig. 9d) serve to reload these faults (red regions). This is the easiest to see by focusing on the

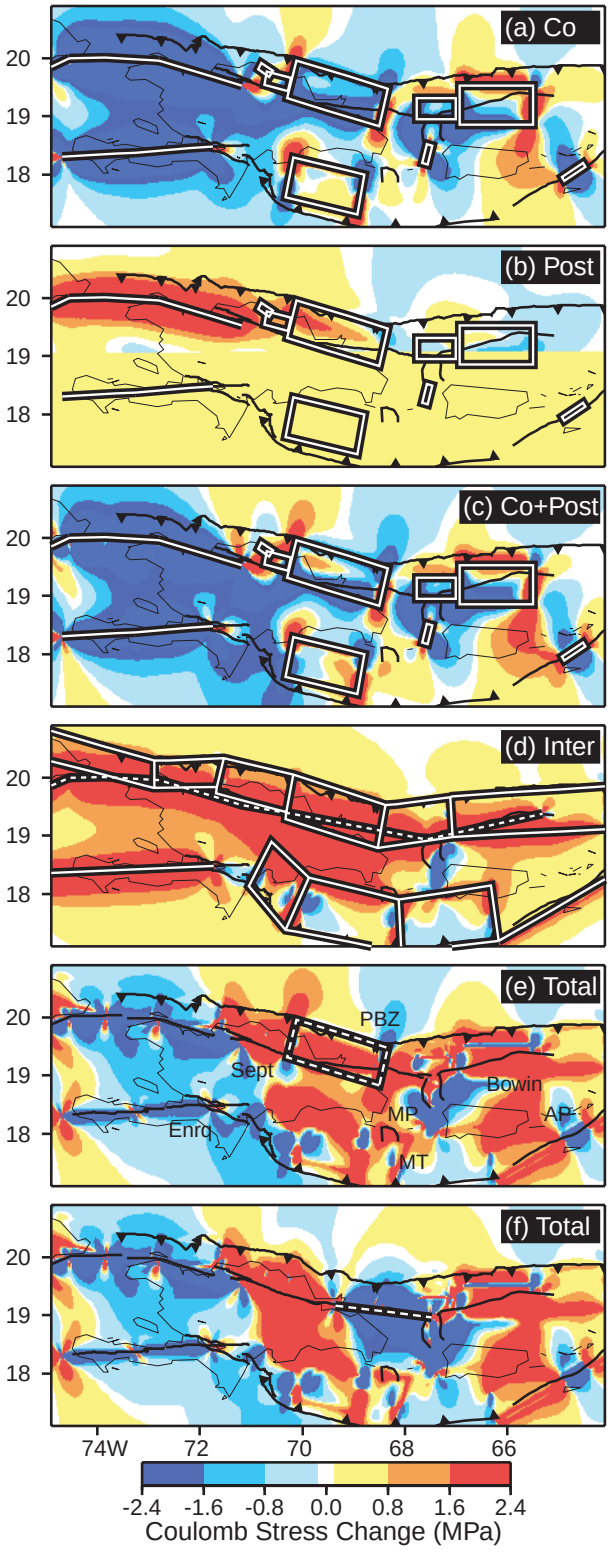

Figure 9. Cumulative Coulomb stress changes resolved on N95°E striking left-lateral strike-slip faults from 1751 to 2007 due to (a) coseismic, (b) postseismic, (c) combined coseismic and postseismic, (d) interseismic and (e) coseismic plus postseismic plus interseismic deformation. (f) Shows how the net stress change (e) is modified if the 1946 earthquake occurred on the eastern Septentrional fault (rupture plane outlined in panel) (Russo & Villasenor 1995), as opposed to occurring on the megathrust. Stresses are resolved at a depth of 15 km with a friction of 0.2. Fault labels are same as in Fig. 5.

Enriquillo fault (longitudes 72°–75°W) in these figures, where large strike-slip earthquakes have occurred. The dominance of Coulomb stress decreases (blue regions) in Fig. 9c shows that coseismic stress relief is stronger than postseismic reloading. However, with the addition interseismic loading the cumulative stress relief since 1751 significantly erodes away (note thin blue line directly under most of the Enriquillo fault in Fig. 9e). This suggests that the fault is within decades of recovering to pre-earthquake stress levels. In contrast, the western Septentrional fault (longitudes 71°–75°W) experiences a complex net stress change pattern (the fault experiences both net stress increases and decreases), as shown in Fig. 9e. To first order, however, the western Septentrional fault currently appears to be neutrally loaded and may not represent a significant source of seismic hazard for the next several decades.

The total change in stress over the past 250 yr has lead to a large build-up of left-lateral shear stress in the location of the central and eastern Septentrional fault (longitudes 68°–71°, Fig. 9e). Stress has accumulated here primarily from interseismic stressing and partly from coseismic slip and postseismic relaxation, following the 1842 earthquake. In addition, this segment has not experienced any significant earthquake over the past 770–960 yr (Prentice *et al.* 2003). However, Russo & Villasenor (1995) have suggested that the 1946 earthquake in this region (Figs 5i and 6i) may have actually ruptured the eastern, offshore part of the Septentrional, as opposed to the megathrust. Although this interpretation is at odds with the aftershock distribution from the 1946 event (Dolan & Wald 1998), we consider an alternative model where the earthquake occurred on the eastern Septentrional fault, offshore of Hispaniola (as there is no evidence of rupture onshore). This alternate earthquake was modelled as being 200 km long, with 5 m of uniform left-lateral slip, consistent with Russo and Villasenor's estimated magnitude (M_S7.8) and empirical scaling laws. Fig. 9f shows how this alternative 1946 rupture model results in significant stress relief on that portion of the Septentrional fault, but leaves high unrelieved stress (as much as 15.0 MPa) on the central portion of the fault to the west (longitudes 69.5°–71°). High stress accumulation (as high as 10.0 MPa) also remains on the Bowin fault (longitudes 65°–67°) due to a lack of a large historical event.

Fig. 10 shows the cumulative Coulomb stress changes as resolved on oblique (rake 67.5°) thrust faults roughly parallel to the Puerto Rico Trench incurred since 1751 from each of the three mechanisms of the earthquake cycle both individually and combined. Each of these panels is accompanied by a smaller subpanel showing stress changes as a function of depth along a cross-section (A–A′) that cuts through the rupture planes associated with the 1751a and 1946 events. These results show that thrust earthquakes (Fig. 10a) work to relieve stress whereas interseismic processes (Fig. 10d) reload the faults. It is interesting to note that interseismic loading of the thrust components of faults in this region (Fig. 10d) are not as significant as that of interseismic loading of strike-slip components (Fig. 9d), owing to the significant obliqueness of subduction along the northeastern Caribbean boundary.

The role of postseismic relaxation in the evolution of Coulomb stress on the thrust component of earthquakes (Fig. 10b) is more complicated than that associated with strike-slip events (Fig. 9b). Postseismic relaxation of a viscoelastic mantle, following thrust events works to both unload and reload different regions of the rupture surfaces, whereas relaxation following strike-slip events only serves to reload these faults. This makes for a complex pattern of combined stress changes on thrust faults when coseismic and postseismic (Fig. 10c) or all three processes (Fig. 10e) are combined. The result is that individual segments are not easily characterized

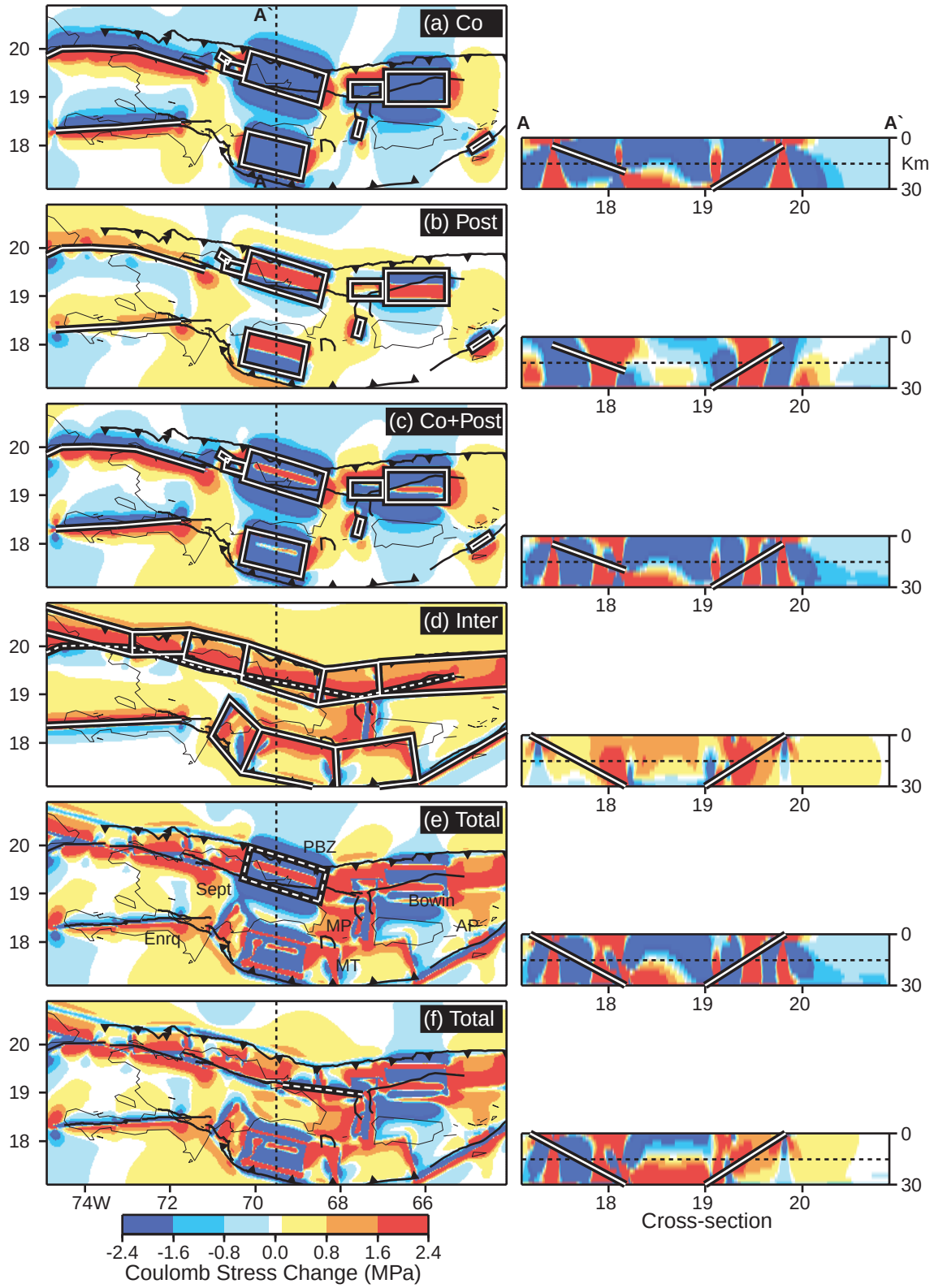

Figure 10. Cumulative Coulomb stress changes resolved on N95°E striking oblique (rake of 67.5°) thrust faults from 1751 to 2007 due to (a) coseismic, (b) postseismic, (c) combined coseismic and postseismic, (d) interseismic and (e) coseismic plus postseismic plus interseismic mechanisms. (f) Shows how the net stress change (e) is modified if the 1946 earthquake occurred on the eastern Septentrional fault (rupture plane outlined in panel, Russo & Villasenor 1995), as opposed to occurring on the megathrust. Stresses are resolved at a depth of 15 km with a friction of 0.8. Fault labels are same as in Fig. 5.

as having experienced a net increase or decrease in Coulomb stress over the past 250 yr. This complexity may contribute to the observation that many megathrust events (such as 1943, 1953 and 2003 earthquakes) do not completely rupture through the depth of the seismogenic zone.

A broad view of the net change in Coulomb stress over the past 250 yr toward thrust earthquakes in the Caribbean (Fig. 10e) suggests that high levels of stress have accumulated on the western portion of the megathrust, west of the edge of the 1946 event (70°W). Although no major earthquake has been documented on this section of the Caribbean–North America plate boundary, there is ample evidence for active reverse faulting along the northern Hispaniola margin and for actively growing folds in the narrow sedimentary wedge at the toe of the margin slope (e.g. Dillon *et al.* 1987, 1992; Calais & de Lépinay 1995).

Calculations also suggest high unrelieved stress in the seismic gap between the 1943 and 1946 events (67.5°–68.5°W) and on the shallow portion of the megathrust above the 1943 rupture zone (67.0°–67.5°W), assuming it only broke the deeper part of the seismogenic zone. Calculated high stress accumulation in these regions changes significantly if the 1946 event was not on the megathrust but instead occurred on the Septentrional fault (Fig. 10f). In this case, high stresses on the vacated 1946 rupture surface becomes a prime target for an earthquake, although there no longer exists a seismic gap between the 1946 and 1943 ruptures. The other region of high accumulated stress for thrust faulting occurs to the east of the 1787 rupture surface (east of 65.5°W) where no large historic earthquakes have been documented (McCann 1985). While this could suggest a region of current seismic potential, the lack of GPS constraints in the region could have led to an overestimation of coupling ratios in the block model, further leading to an overestimation of interseismic loading.

5 SUMMARY AND CONCLUSIONS

This study shows how active faults in the northeastern Caribbean communicate and influence each other through Coulomb stress changes. All of the fault systems are interseismically loaded by the regional tectonics associated with the oblique subduction and associated strain partitioning between the Caribbean and North American plates. We find that coseismic stress changes often encourage subsequent events. For instance, the observed westward propagation of earthquakes on the Septentrional Fault (1842, 1887), the Enriquillo Fault (1751b, 1770) and along the megathrust (1787, 1943, 1946, 1953, 2003) were all encouraged by coseismic Coulomb stress changes greater than 0.1 MPa associated with the earlier events in each sequence. Stress changes associated with postseismic relaxation of a viscoelastic mantle serves to reload strike-slip rupture surfaces above, after an earthquake. However, reloading of megathrust rupture surfaces due to postseismic relaxation is more complex, with stress on some areas of the rupture surface increasing, while decreasing on others. This difference, associated with differences in the distribution of coseismic stress changes with depth between a vertical strike-slip fault and a shallow dipping thrust fault extends to the loading of neighbouring segments after each type of earthquake. After strike-slip earthquakes, postseismic relaxation always increases Coulomb stress on neighbouring segments, encouraging earthquake sequences. In contrast, postseismic relaxation appears to either unload or neutrally load neighbouring thrust segments.

We also find that on the Caribbean plate, earthquakes within one fault system can encourage or discourage events on the other fault systems. For example, earthquakes on the Septentrional strike-slip fault relieve a small level of stress on the subparallel Enriquillo fault to the south. This stress relief is further magnified by postseismic relaxation. The relationship also works in the opposite direction, with earthquakes and postseismic relaxation on the Enriquillo fault leading to modest unloading of the Septentrional fault. Over many earthquake cycles, it is not hard to imagine that this stress communication is responsible for the apparent observed anticorrelation of events on these respective fault systems, with earthquakes on the Enriquillo fault having occurred in the 18th and on the Septentrional fault in the 19th century. Strike-slip events on the Septentrional and Bowin faults also serve to relieve shear on the North American/Caribbean megathrust. This may explain why no earthquakes in the past 250 yr have been observed on the megathrust west of 70°W. However, it should also be noted that this is the region where the megathrust terminates, and hence, the earthquake potential here is uncertain.

This analysis also suffers from a number of limitations, such as uncertainties in the location and source mechanism of some historical earthquakes, viscoelastic relaxation occurring only in the mantle and without consideration as to the influence of the subducting slab, assumption of uniform coseismic slip and uncertainties in the block model used to calculate interseismic stresses due to limited GPS constraints. Our results, nevertheless, provide a quantitative view of the evolution of stress on the Caribbean plate due to coseismic, postseismic, and interseismic processes. The location of unrelieved Coulomb stress on active faults may especially be indicative of the regions where seismic hazards are currently the greatest. The greatest net build-up of Coulomb stress changes over the past 250 yr occurs along the central and eastern segment of the Septentrional and the Bowin strike-slip faults (65°–71°W), as no recent earthquake has relieved stress in these regions. This would not be the case if the 1946 earthquake actually occurred on the eastern Septentrional fault as opposed to the megathrust. In this scenario, unrelieved stress on the Septentrional fault would be isolated to the central Septentrional between 69°–71°W. For oblique thrust faults, net stress build-up over the past 250 yr is largest on the North American/Caribbean megathrust west of 70.5°W. This high accumulated stress region starts further east at 69.5°W if the 1946 event occurred on the Septentrional fault. High Coulomb stress has also developed east of 65.5°W (edge of 1787 quake), where no historic events have been inferred to have relieved stress. Because of limited GPS measurements in this region from which to constrain the block model, interseismic fault slip rates and hence stressing rates may have been over-estimated. In this case, seismic hazard in this region would be much reduced.

ACKNOWLEDGMENT

This research was supported by grant #EAR-0409487 from the National Science Foundation. We thank two anonymous reviewers for helpful suggestions that improved the manuscript.

REFERENCES

Byrne, D.B., Suarez, G. & McCann, W.R., 1985. Muertos Trough subduction – microplate tectonics in the northern Caribbean, *Nature*, **317,** 420–421.

Calais, E. & de Lépinay, B.M., 1995. Strike-slip tectonic processes in the northern Caribbean between Cuba and Hispaniola (Windward Passage), *Mar. Geophys. Res.*, **17**(1), 63–95.

Calais, E., Mazabraud, Y., de Lapinay, B.M., Mann, p., Mattioli, G. & Jansma, P., 2002. Strain partitioning and fault slip rates in the northeastern Caribbean from GPS measurements, *Geophys. Res. Lett.*, **29,** doi:10.1029/2002GL015397.

Casarotti, E. & Piersanti, A., 2003. Postseismic stress diffusion in Chile and South Peru, *Earth planet. Sci. Lett.*, **206,** 325–333.

Chery, J., Carretier, S. & Ritz, J.F., 2001. Postseismic stress transfer explains time clustering of large earthquakes in Mongolia, *Earth planet. Sci. Lett.*, **194,** 277–286.

Collettini, C. & Sibson, R.H., 2001. Normal faults, normal friction?, *Geology*, **29,** 927–930.

DeMets, C., Jansma. P.E., Mattioli, G.S., Dixon, T.H., Farina, F., Bilham, R., Calais, E. & Mann, P., 2000. GPS geodetic constraints on Caribbean-North America plate motion, *Geophys. Res. Lett.*, **27,** 437–440.

Deng, J. & Sykes, L.R., 1997. Evolution of the stress field in southern California and triggering of moderate-size earthquakes: a 200-year perspective, *J. geophys. Res.*, **102,** 9859–9886.

Dillon, W.P., Scanlon, K.M., Edgar, N.T. & Parson, L.M., 1987. Pattern of growth folding at northern Caribbean plate boundary north of western Hispaniola, as disclosed by long-range side-scan sonar, *Am. Assoc. Petrol. Geol. Bull.*, **71**(5), 548.

Dillon, W.P., Austin, J.A., Jr., Scanlon, K.M. & Coleman, D.F., 1992. Structure and development of the insular margin north of western Hispaniola: a tectonic accretionary wedge on the Caribbean plate boundary, *Mar. Petrol. Geol.*, **9,** 70–88.

Dixon, T.H., Farina, F., DeMets, C., Jansma, P., Mann, P. & Calais, E. 1998. Relative motion between the Caribbean and North American plates and related boundary zone deformation from a decade of GPS observations, *J. geophys. Res.*, **103,** 15 157–15 182.

Dolan, J.F. & Bowman, D.D., 2004. Tectonic and seismologic setting of the 22 September 2003, Puerto Plata, Dominican Republic earthquake: implications for earthquake hazard in northern Hispaniola, *Seism. Res. Lett.* **75,** 587–597.

Dolan, J.F. & Wald, D.J., 1998. 1943–1953 north-central Caribbean earthquakes, *Geol. Soc. Am., Spec. Pap.* **326,** 143–169.

Dolan, J.F., Mullins, H.T. & Wald, D.J., 1998. Active tectonics of the north-central Caribbean: oblique collision, strain partitioning, and opposing subducted slabs, *Geol. Soc. Am., Spec. Pap.* **326,** 1–61.

Doser, D.I., Rodriguez, M. & Flores, C., 2005. Historical earthquakes of Puerto Rico-Virgin Islands region (1915–1963), *Geol. Soc. Am., Spec Pap.* **385,** 103–114.

Freed, A.M., 2005. Earthquake triggering by static, dynamic, and postseismic stress transfer, *Ann. Rev. Earth Planet. Sci.*, **33,** 335–367.

Freed, A.M. & Lin, J., 1998. Time-dependent changes in failure stress following thrust earthquakes, *J. geophys. Res.*, **103,** 24 393–424 10.

Freed, A.M. & Lin, J., 2001. Delayed triggering of the 1999 Hector Mine earthquake by viscoelastic stress transfer, *Nature*, **411,** 180–183.

Freed, A.M., Ali, S.T. & Bürgmann, R., 2007. Evolution of stress in Southern California for the past 200 years from coseismic, postseismic and interseismic stress changes, *J. geophys. Res.*, **169,** 1164–1179.

Fujii, Y. & Matsu'ura, M., 2000. Regional difference in scaling laws for large earthquakes and its tectonic implication, *Pure appl. Geophys.*, **157,** 2283–2302.

Grindlay, N.R., Mann, P., Dolan, J.F. & van Gestel, J.P., 2005. Neotectonics and subsidence of northern Puerto Rico-Virgin Islands margin in response to the oblique subduction of high standing ridges, *Geol. Soc. Am., Spec. Pap.* **385,** 31–60.

Gomberg, J., 1996. Stress/strain changes and triggered seismicity following the M_w7.3 Landers, California, earthquake, *J. geophys. Res.*, **101,** 751–764.

Gomberg, J., Bodin, P. & Reasenberg, P.A., 2003. Observing earthquakes triggered in the near field by dynamic deformations, *Bull. seism. Soc. Am.*, **93,** 118–138.

Gutenberg, B. & Richter, C.F., 1954. *Seismicity of the Earth and Associated Phenomena*, Princeton University Press, Princeton, New Jersey.

Hardebeck, J.L., Nazareth, J.J. & Hauksson, E., 1998. The static stress change triggering model; constraints from two southern California aftershock sequences, *J. geophys. Res.*, **103,** 24 427–24 437.

Harris, R.A. & Simpson, R.W., 1996. In the shadow of 1857: the effect of the great Ft. Tejon earthquake on subsequent earthquakes in southern California, *Geophys. Res. Lett.* **23,** 229–232.

Harris, R.A. & Simpson, R.W., 1998. Suppression of large earthquakes by stress shadows; a comparison of Coulomb and rate-and-state failure, *J. geophys. Res.* **103,** 24 439–24 451.

Hodgkinson, K.M., Stein, R.S. & Marshall, G., 1996. The 1954 Rainbow Mountain-Fairview Peak-Dixie Valley earthquake sequences: a triggered normal faulting sequence, *J. geophys. Res.*, **101,** 25 459–25 472.

Hu, Y., Wang, K., He, J., Klotz, J. & Khazaradze, G., 2004. Three-dimensional viscoelastic finite element model for post- seismic deformation of the great 1960 Chile earthquake, *J. geophys. Res.*, **109,** doi:10.1029/2004JB003163.

Hyodo, M. & Hirahara, K., 2004. GeoFEM kinematic earthquake cycle simulation in Southwest Japan, *Pure appl. Geophysics*, **161,** 2069–2090.

Jaeger, J.C. & Cook, N.G., 1979. *Fundamentals of Rock Mechanics*, 3rd edn, Chapman & Hall, London.

Jansma, P.E. & Mattioli, G.S., 2005. GPS results from Puerto Rico and the Virgin Islands: constraints on tectonic setting and rates of active faulting, *Geol. Soc. Am., Spec. Pap.* **385,** 13–30.

Jansma, P.E., Mattioli, G.S. Lopez, A., DeMets, C., Dixon, T.H., Mann, P. & Calais, E., 2000. Neotectonics of Puerto Rico and the Virgin Islands, northeastern Caribbean, from GPS geodesy, *Tectonics*, **19,** 1021–1037.

Kelleher, J., Sykes, L. & Oliver, J., 1973. Possible criteria for predicting earthquake locations and their application for major plate boundaries of the Pacific and the Caribbean, *J. geophys. Res.*, **78,** 2547–2585.

Khazaradze, G., Wang, K., Klotz, J., Hu, Y. & He, J., 2002. Prolonged post-seismic deformation of the 1960 great Chile earthquake and implications for mantle rheology, *Geophys. Res. Lett.*, **29,** doi:10.1029/2002GL015986.

King, G.C.P. & Cocco, M., 2001. Fault interactions by elastic stress changes: new clues from earthquake sequences. *Adv. Geophys.*, **44,** 1–38.

King, G.C.P., Stein, R.S. & Lin, J., 1994. Static stress changes and triggering of earthquakes, *Bull. seism. Soc. Am.*, **84,** 935–953.

Ladd, J.W., Vonhuene, R.E. & Watkins, J.S., 1977. Seismic-reflection profiles over continental margin of Guatemala, *AGU Trans.*, **58,** 1150.

Lin, J. & Stein, R.S., 2004. Stress triggering in thrust and subduction earthquakes and stress interaction between the southern San Andreas and nearby thrust and strike-slip faults, *J. geophys. Res.*, **109,** doi:10.1029/2003JB002607.

Lithgow, C.W., McCann, W.R. & Joyce, J., 1987. Extensional tectonics at the eastern edge of the Puerto Rico platelet, *EOS Trans.*, **68,** 466–489.

Lorenzo-Martin, F., Roth, F. & Wang, R.J., 2006. Inversion for rheological parameters from postseismic surface deformation associated with the 1960 Valdivia earthquake, Chile, *Geophys. J. Int.*, **164,** 75–87.

Manaker, D.M. *et al.*, 2008. Interseismic Plate coupling and strain partitioning in the Northeastern Caribbean, *Geophys. J. Int.*, **174,** 889–903.

Mann, P., Prentice, C.S., Burr, G., Peña, L.R. & Taylor, F.W., 1998. Tectonic geomorphology and paleoseismology of the Septentrional fault system, Dominican Republic, *Geol. Soc. Am., Spec. Pap.* **326,** 63–124.

Mann, P., Calais, E., Ruegg, J.C., DeMets, C., Jansma, P.E. & Mattioli, G.S., 2002. Oblique collision in the northeastern Caribbean from GPS measurements and geological observations, *Tectonics*, **21,** doi:10.1029/2001TC001304.

Marsan, D. & Bean, C.J., 2003. Seismicity response to stress perturbations, analyzed for a worldwide catalogue, *Geophys. J. Int.*, **154,** 179–195.

Masson, D.G. & Scanlon, K.M., 1991. The neotectonic setting of Puerto-Rico, *Geol. Soc. Am. Bull.*, **103,** 144–154.

McCann, W.R., 1985. On the earthquake hazards of Puerto-Rico and the Virgin Islands, *Bull. seism. Soc Am.*, **75,** 251–262.

McCann, W.R., 2006. Estimating the threat of tsunamogenic earthquakes and earthquake induced landslide tsunami in the Caribbean, *Carribbean Tsunami Hazard*, pp. 43–65, eds Aurelio, M. & Philip, L., World Scientific Publishing, Singapore.

McCann, W.R. & Sykes, L.R., 1984. Subduction of aseismic ridges beneath the Caribbean plate – implications for the tectonics and seismic potential of the Northeastern Caribbean, *J. geophys. Res.*, **89,** 4493–4519.

Nalbant, S.S., Hubert, A. & King, G.C.P., 1998. Stress coupling between earthquakes in northwest Turkey and the north Aegean Sea, *J. geophys. Res.*, **103,** 24 469–24 486.

Nostro, C., Cocco, M. & Belardinelli, M.E., 1997. Static stress changes in extensional regimes: an application to southern Apennines (Italy), *Bull. seism. Soc. Am.*, **87,** 234–248.

Pacheco, J.F. & Sykes, L.R., 1992. Seismic moment catalog of large shallow earthquakes, *1900 to 1989*, *Bull. seism. Soc. Am.*, **82,** 1306–1349.

Parsons, T., Stein R.S., Simpson, R.W. & Reasenberg, P.A. 1999. Stress sensitivity of fault seismicity: a comparison between limited-offset oblique and major strike-slip faults, *J. geophys. Res.* **104,** 20 183–20 202.

Pollitz, F.F., 1996. Coseismic deformation from earthquake faulting on a layered spherical Earth, *Geophys. J. Int.*, **125,** 1–14.

Pollitz, F.F., 1997. Gravitational viscoelastic postseismic relaxation on a layered spherical Earth, *J. geophys. Res.*, **102,** 17 921–17 941.

Pollitz, F.F. & Nyst, M., 2005. A physical model for strain accumulation in the San Francisco Bay Region, *Geophys. J. Int.*, **160,** 302–317.

Pollitz, F.F. & Sacks, I.S., 1995. Consequences of stress changes following the 1891 Nobi earthquake, Japan, *Bull. Seismol. Soc. Am.*, **85,** 796–807.

Pollitz, F.F. & Sacks, I.S., 1997. The 1995 Kobe, Japan, earthquake: a long-delayed aftershock of the offshore 1944 Tonankai and 1946 Nankaido earthquakes, *Bull. seism. Soc. Am.*, **87,** 1–10.

Pollitz, F.F. & Sacks, I.S., 2002. Stress triggering of the 1999 Hector Mine earthquake by transient deformation following the 1992 Landers earthquake, *Bull. seism. Soc. Am.*, **87,** 1–10.

Pollitz, F.F., Vergnolle, M. & Calais, E., 2003. Fault interaction and stress triggering of 20th century earthquakes in Mongolia, *J. geophys. Res.*, **108,** doi:10.1029/2002JB002375.

Prentice, C.S., Mann, P., Pena, L.R., & Burr, G., 2003. Slip rate and earthquake recurrence along the central Septentrional fault, North American-Caribbean plate boundary, Dominican Republic, *J. geophys. Res.*, **108,** doi:10.1029/2001JB000442.

Reasenberg, P.A. & Simpson, R.W., 1992. Response of regional seismicity to the static stress change produced by the Loma Prieta earthquake, *U.S. Geol. Surv. Prof. Pap.* **1550-D,** 49–72.

Reid, H.F. & Taber, S., 1919. The Porto Rico earthquakes of October November, *1918*, *Bull. seism. Soc. Am.*, **9,** 95–127.

Reid, H.F. & Taber, S., 1920. The Virgin Islands earthquakes of 1867–1868, *Bull. seism. Soc. Am.*, **10,** 9–30.

Robinson, R. & Benites, R., 1995. Synthetic seismicity models of multiple interacting faults, *J. geophys. Res.*, **100,** 18 229–18 238.

Rothe, J.P., 1969. *The Seismicity of the Earth, 1953–1965*, Vol. 336, UNESCO, Paris.

Russo, R.M. & Villasenor, A., 1995. The 1946 Hispaniola earthquake and the tectonics of North America-Caribbean plate boundary zone, northeast Hispaniola, *J. geophys. Res.*, **100,** 6265–6280.

Salterain, P., 1883. Ligera resena de los tremblores de tierra ocurridos en la isla de Cuba (The earthquakes of the Island of Cuba): Boletin de la Comision del Mapa, *Geologico de Espana*, **10,** 371–385.

Savage, J.C., 1983. A dislocation model of strain accumulation and release at a subduction zone, *J. geophys. Res.*, **88,** 4984–4996.

Scherer, J., 1912. Great earthquakes in the island of Haiti, *Bull. seism. Soc. Am.*, **2,** 161–180.

Scholz, C.H., 2002. The Mechanics of Earthquakes and Faulting, Cambridge University Pres, Cambridge.

Scholz, C.H., 1998. Earthquakes and friction laws, *Nature*, **391,** 37–42.

Scordilis, E.M., 2006. Empirical global relations converting Ms and Mb to moment magnitude, *J. Seism.*, **10,** 225–236.

Shearer, P.M., 1997. Improving local earthquake locations using the L1 norm and waveform cross correlation: application to the Whittier Narrows, California, aftershock sequence, *J. geophys. Res.*, **102,** 8269–8283.

Smith, B.R. & Sandwell, D.T., 2006. A model of the earthquake cycle along the San Andreas Fault system for the past 1000 years, *J. geophys. Res.*, **111,** doi:10.1029/2005JB003703.

Stein, R.S., 1999. The role of stress transfer in earthquake occurrence, *Nature*, **402,** 605–609.

Stein, R.S., 2003. Earthquake Conversations, *Scient. Am.*, **288,** 72–79.

Stein, R.S. & Ekstrom, G., 1992. Seismicity and geometry of a 110-km long blind thrust fault, 2, Synthesis of the 1982–85 California earthquake sequence, *J. geophys. Res.*, **97,** 4865–4883.

Stein, R.S. & Lisowski, M., 1983. The 1979 Homestead Valley earthquake sequence, California: control of aftershocks and postseismic deformation, *J. geophys. Res.* **88,** 6477–6490.

Stein, R.S., King, G.C.P. & Lin, J., 1994. Stress triggering of the 1994 M = 6.7 Northridge, California earthquake by its predecessors, *Science*, **265,** 1432–1435.

Stein, R.S., Barka, A.A. & Dietrich, J.H., 1997. Progressive failure on the North Anatolian fault since 1939 by earthquake stress triggering, *Geophys. J. Int.*, **128,** 594–604.

Taber, S., 1922. The great fault troughs of the Antilles, *J. Geol.* **30,** 89–114.

Tanner, J.G. & Shepherd, J.B., 1997. Project catalogue and seismic hazard maps, seismic hazard in Latin America and the Caribbean, *Panamerican Inst. Geogr. History*, **1,** 143 pp.

Taylor, M.A.J., Dmowska, R. & Rice, J.R., 1998. Upper plate stressing and seismicity in the subduction earthquake cycle, *J. geophys. Res.*, **103,** 24 523–24 552.

tenBrink, U. & Lin, J., 2004. Stress interaction between subduction earthquakes and forearc strike-slip faults: modeling and application to the Northern Caribbean plate boundary, *J. geophys. Res.*, **109,** B12310, doi:10.1029/2004JB003031.

Toda, S. & Stein, R.S., 2002. Response of the San Andreas Fault to the 1983 Coalinga–Nuñez Earthquakes: An Application of Interaction-based Probabilities for Parkfield, *J. geophys. Res.*, **107,** doi:10.1029/2001JB000172.

Toda, S., Stein, R.S., Reasenberg, P.A. Dieterich, J.H. & Yoshida, A., 1998. Stress transferred by the 1995 Mw = 6.9 Kobe, Japan, shock: effect on aftershocks and future earthquake probabilities, *J. geophys. Res.*, **103,** 24 543–24 565.

vanGestel, J.P., 1998. Structure and tectonics of the upper Cenozoic Puerto Rico Virgin Islands carbonate platform as determined from seismic reflection studies, *J. geophys. Res.*, **103,** 30 505–30 530.

Wang, K., He, J., Dragert, H. & James, T.H., 2001. Three-dimensional viscoelastic interseismic deformation model for the Cascadia subduction zone, *Earth Planets Space*, **53,** 295–306.

Wells, D.L. & Coppersmith, K.J., 1994. New empirical relationships among magnitude, rupture length, rupture width, rupture area, and surface displacement, *Bull. seism. Soc. Am.*, **84,** 974–1002.

Wyss, M. & Wiemer, S., 2000. Change in the probability for earthquakes in southern California due to the Landers magnitude 7.3 earthquake, *Science*, **290,** 1334–1338.

Zeng, Y., 2001. Viscoelastic stress-triggering of the 1999 Hector Mine earthquake by the 1992 Landers earthquake, *Geophys. Res. Lett.*, **28,** 3007–3010.

Zoback, M.D. *et al*., 1987. New evidence on the state of stress of the San Andreas fault system, *Science*, **238,** 1105–1111.